

Hydrodynamics and multiscale order in confluent epithelia

Josep-Maria Armengol-Collado,^{1,*} Livio N. Carenza,^{1,*} and Luca Giomi^{1,†}

¹*Instituut-Lorentz, Universiteit Leiden, P.O. Box 9506, 2300 RA Leiden, The Netherlands*

We formulate a hydrodynamic theory of confluent epithelia: i.e. monolayers of epithelial cells adhering to each other without gaps. Taking advantage of recent progresses toward establishing a general hydrodynamic theory of p -atic liquid crystals, we demonstrate that collectively migrating epithelia feature both nematic (i.e. $p = 2$) and hexatic (i.e. $p = 6$) order, with the former being dominant at large and the latter at small length scales. Such a remarkable multiscale liquid crystal order leaves a distinct signature in the system's structure factor, which exhibits two different power law scaling regimes, reflecting both the hexagonal geometry of small cells clusters, as well as the uniaxial structure of the global cellular flow. In the overdamped regime, that is when viscous forces are negligible compared to the frictional forces arising from the interaction with the substrate, the predictions of our hydrodynamic theory are in excellent agreement with the outcome of the Self-Propelled Voronoi model of confluent epithelial layers.

Collective cell migration – that is, the ability of multicellular systems to cooperatively flow, even in the absence of a central control mechanism – has surged, in the past decade, as one of the central questions in cell biology and tissue biophysics [1]. Whether spreading on a synthetic substrate [2] or invading the extracellular matrix (ECM) [3], multicellular systems can move coherently within their micro-environment and coordinate the dynamics of their actin cytoskeleton, while retaining cell-cell contacts. This ability lies at the heart of a myriad of processes that are instrumental for life, such as embryonic morphogenesis and wound healing, but also of life-threatening conditions, such as metastatic cancer.

Understanding the physical origin of this behavior inevitably demands reliable theoretical models, aimed at providing a conceptual framework for dissecting and deciphering the wealth of biophysical data stemming from *in vitro* experiments and *in vivo* observations. Following the pioneering works by Nagai and Honda [4], Farhadifar *et al.* [5], Bi *et al.* [6, 7] and others (e.g. Refs. [8–11]), *cell-resolved* models have played so far the leading role in this endeavour. Taking inspiration from the physics of foams (see e.g. Refs. [12, 13]), these models portray a confluent tissue as a collection of adjacent polygonal cells (Fig. 1a), characterized by a simple quadratic energy involving exclusively geometrical quantities: i.e.

$$E = \sum_{c \in \text{cells}} \left[K_A (A_c - A_0)^2 + K_P (P_c - P_0)^2 \right]. \quad (1)$$

The first term in Eq. (1), with A_c the cell area, embodies a combination cells' volumetric incompressibility and monolayer resistance to thickness fluctuations. The second term, involving the cell perimeter P_c , results from the cytoskeletal contractility (quadratic in P_c) and the effective interfacial tension due to cell-cell adhesion and cortical tension (both linear in P_c) [5]. The constants

A_0 and P_0 represent, respectively, the preferred area and perimeter of each cell. The dynamics of the tissue is then assumed to be governed by a set of overdamped Langevin equations, expressing the interplay between cells' autonomous motion and the remodelling events that underlie the tissue's collective dynamics. An especially efficient model in this class is the so called Self-Propelled Voronoi model (SPV) [7], where cells are approximated as plane-tiling Voronoi polygons [14], whose state is entirely described by the two-dimensional vectors \mathbf{r}_c and \mathbf{p}_c representing, respectively, the position and the direction of motion of the c -th cell. That is

$$\frac{d\mathbf{r}_c}{dt} = v_0 \mathbf{p}_c - \mu \nabla_{\mathbf{r}_c} E, \quad \frac{d\mathbf{p}_c}{dt} = \eta_c \mathbf{p}_c^\perp, \quad (2)$$

where v_0 is the cell's self-propulsion speed and μ is the mobility coefficient. The quantity η_c is a random number with zero mean and correlation function $\langle \eta_c(t) \eta_{c'}(t') \rangle = 2\mathcal{D}_r \delta_{cc'} \delta(t - t')$, with \mathcal{D}_r a rotational diffusion coefficient, whereas $\mathbf{p}_c^\perp \cdot \mathbf{p}_c = 0$. Despite their conceptual simplicity, cell-resolved models agree remarkably well with experimental data on confluent monolayers (see e.g. Refs. [15, 16]). In particular, as shown by Bi *et al.*, they account for a solid-to-liquid transition governed exclusively by a dimensionless shape target parameter, $p_0 = P_0 / \sqrt{A_0}$, embodying the spontaneous degree of acircularity of individual cells [7].

Furthermore, Pica Ciamarra and coworkers have demonstrated that, as in the case of two-dimensional melting, the solid and isotropic liquid states of these model-epithelia are separated by an intermediate *hexatic* phase, in which the system exhibits the typical 6-fold rotational symmetry of two-dimensional crystals and yet is able to flow (Fig. 1b and Refs. [17, 18]). Shortly after discovery, the same property has been recovered within the framework of the cellular Potts model, thereby strengthening the idea that hexatic order may in fact serve as a guiding principle to unravel the collective dynamics of confluent epithelia [19].

In addition to providing a powerful tool to conceptualize experimental data, cell-resolved models have prompted the development of continuum *coarse-grained*

* These authors contributed equally.

† giomi@lorentz.leidenuniv.nl

models, aimed at describing the collective dynamics of multicellular systems at a larger length scale, encompassing multiple coherently moving cells. These models, in turn, can be schematically grouped in two categories: 1) models based on (isotropic/polar/nematic) active gels (see e.g. Refs. [20–22]); 2) models built around the, so called, shape-tensor (see e.g. Refs. [23–26]), i.e. a rank-2 tensor, similar to the inertia tensor in kinematics, that embodies the geometrical structure of the polygonal cells. Although both classes of models hold great heuristic value and represent a solid foundation for any future development, they suffer from the same limitation: being based on a tensorial order parameter whose rank is two or less, these models can account at most for 2-fold rotational symmetry (i.e. nematic order). The latter is prominent in specific multicellular systems consisting of elongated cells (see e.g. Refs. [27, 28]), but can hardly be regarded as a general feature of epithelia and, despite its growing use in the interpretation of experimental data, its existence has remained elusive in cell-resolved models [29–31].

Motivated by these recent discoveries, in this Letter we propose a continuum theory of confluent epithelia rooted in the hydrodynamics of liquid crystals with generic p -atic rotational symmetry (hereafter p -atic liquid crystals). To this end, we exploit preliminary work toward extending the classic hydrodynamic theory of hexatic liquid crystals [32, 33] to account for arbitrary discrete rotational symmetry [34, 35]. Our analysis suggests that collectively migrating epithelial layers, such as that theoretically depicted by the SPV model in Eqs. (1) and (2), feature neither purely nematic (i.e. $p = 2$) nor purely hexatic (i.e. $p = 6$) order, but a remarkable scale-dependent combination of both, thereby organizing in what we will refer to as a *hexanematic* liquid crystal in the following.

The central object in our approach is the rank- p tensor order parameter, $\mathbf{Q}_p = Q_{i_1 i_2 \dots i_p} \mathbf{e}_{i_1} \otimes \mathbf{e}_{i_2} \otimes \dots \otimes \mathbf{e}_{i_p}$ with $i_n = \{x, y\}$ and $n = 1, 2 \dots p$, constructed upon averaging the p -th tensorial power of the local orientation $\mathbf{\nu} = \cos \vartheta \mathbf{e}_x + \sin \vartheta \mathbf{e}_y$, representing a cell's local orientation. That is

$$\mathbf{Q}_p = \sqrt{2^{p-2}} \llbracket \langle \mathbf{\nu}^{\otimes p} \rangle \rrbracket = \sqrt{2^{p-2}} |\Psi_p| \llbracket \mathbf{n}^{\otimes p} \rrbracket, \quad (3)$$

where $\langle \dots \rangle$ denotes the ensemble average, the operator $\llbracket \dots \rrbracket$ has the effect of rendering an arbitrary tensor traceless and symmetric [36]. The vector $\mathbf{n} = \cos \theta \mathbf{e}_x + \sin \theta \mathbf{e}_y$ is the analogue of the director field in standard lexicon of nematic liquid crystals and marks the average cellular direction, which in turn is invariant under rotations of $2\pi/p$. The fields $|\Psi_p|$ and θ , represent respectively the magnitude and phase of the complex p -atic order parameter $\Psi_p = \langle e^{ip\theta} \rangle = |\Psi_p| e^{ip\theta}$, while the normalization factor is chosen so that $|\mathbf{Q}_p|^2 = |\Psi_p|^2/2$ for all p values. For $p = 2$, Eq. (3) readily gives the standard nematic order parameter tensor: i.e. $\mathbf{Q}_2 = |\Psi_2| (\mathbf{n} \otimes \mathbf{n} - \mathbb{1}/2)$, with $\mathbb{1}$ the identity tensor.

The order parameter tensor \mathbf{Q}_p , the mass density ρ

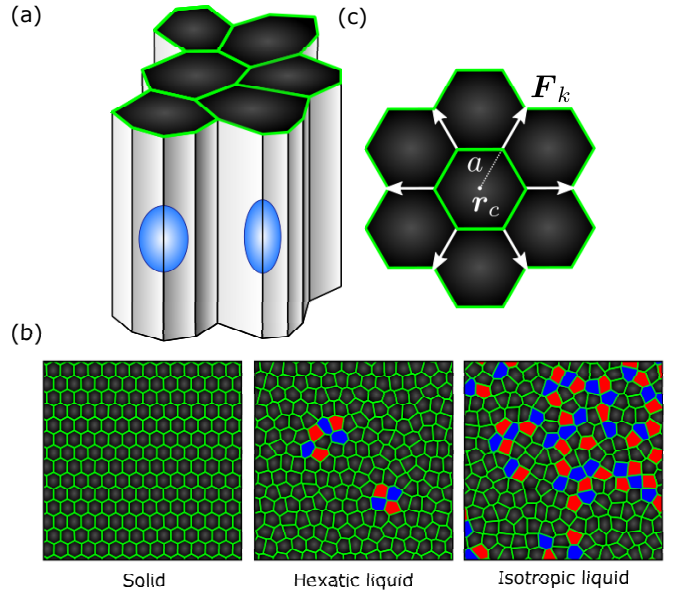


FIG. 1. (a) Schematic representation of confluent epithelial cells. (b) Examples solid, hexatic and isotropic phases obtained from numerical solutions of Eqs. (1) and (2), for $v_0/(\mu K_A A_0^{3/2}) = 0.01$, $\mathcal{D}_r/(\mu K_p) = 1$ and $p_0 = 3.70$, 3.80 and 3.95, respectively. Cells colored in red have 5 neighbors, blue ones have 7 and the others 6. (c) Schematic representation of the 6-fold symmetric force complex exerted by cells.

and the momentum density $\rho \mathbf{v}$, with \mathbf{v} the local velocity field, comprise the set of hydrodynamic variables describing the dynamics of a generic p -atic fluid, which in turn is governed by the following set of partial differential equations [34, 35]:

$$\frac{D\rho}{Dt} + \rho \nabla \cdot \mathbf{v} = \mathcal{D}_0 \nabla^2 \rho, \quad (4a)$$

$$\rho \frac{D\mathbf{v}}{Dt} = \nabla \cdot \boldsymbol{\sigma} + \mathbf{f}, \quad (4b)$$

$$\begin{aligned} \frac{D\mathbf{Q}_p}{Dt} &= \Gamma_p \mathbf{H}_p + p \llbracket \mathbf{Q}_p \cdot \boldsymbol{\omega} \rrbracket + \bar{\lambda}_p \text{tr}(\mathbf{u}) \mathbf{Q}_p \\ &+ \lambda_p \llbracket \nabla^{\otimes p-2} \mathbf{u} \rrbracket + \nu_p \llbracket \nabla^{\otimes p \bmod 2} \mathbf{u}^{\otimes \lfloor p/2 \rfloor} \rrbracket, \end{aligned} \quad (4c)$$

where $D/Dt = \partial_t + \mathbf{v} \cdot \nabla$ is the material derivative, \mathcal{D}_0 is the diffusion coefficient, the rank-2 tensors $\boldsymbol{\omega} = [\nabla \mathbf{v} - (\nabla \mathbf{v})^T]/2$ and $\mathbf{u} = [\nabla \mathbf{v} + (\nabla \mathbf{v})^T]/2$, with T indicating transposition, are the vorticity and strain rate tensors, respectively. Eqs. (4a) and (4b) are the standard mass and momentum conservation equations, with $\boldsymbol{\sigma}$ the stress tensor and \mathbf{f} an arbitrary body force. In Eq. (4c), Γ_p^{-1} is a rotational viscosity and $\mathbf{H}_p = -\delta F/\delta \mathbf{Q}_p$ is the molecular tensor describing the relaxation of the p -atic phase toward the minimum of the free energy F . The dot product in the first line of Eq. (4c) implies a contraction of one index of \mathbf{Q}_p with one of $\boldsymbol{\omega}$: thus $(\mathbf{Q}_p \cdot \boldsymbol{\omega})_{i_1 i_2 \dots i_p} = Q_{i_1 i_2 \dots j} \omega_{j i_p}$. On the second line $(\nabla^{\otimes n})_{i_1 i_2 \dots i_n} = \partial_{i_1} \partial_{i_2} \dots \partial_{i_n}$, while $\llbracket \dots \rrbracket$ denotes the floor function and $p \bmod 2 = p - 2\lfloor p/2 \rfloor$ is zero for

even p values and one for odd p values. Finally, $\bar{\lambda}_p$, λ_p and ν_p are material parameters expressing the strength of the coupling between p -atic order and flow.

Now, in order for Eqs. (4) to account for the dynamics of epithelial cell layers, we must specify the structure of the body force \mathbf{f} in Eq. (4b) and the stress tensor $\boldsymbol{\sigma}$. As cells collectively crawl on a substrate, at a speed of order 1 $\mu\text{m}/\text{h}$, the former can be model as a Stokesian drag: $\mathbf{f} = -\varsigma \mathbf{v}$, with ς a drag coefficient. The latter, on the other hand, is routinely decomposed in three terms: an energy dissipating *viscous* stress $\boldsymbol{\sigma}^{(v)} = 2\eta \mathbf{u} + \zeta \text{tr}(\mathbf{u})$, with η and ζ the shear and bulk viscosity respectively, an energy conserving *reactive* stress $\boldsymbol{\sigma}^{(r)}$ and an energy injecting *active* stress $\boldsymbol{\sigma}^{(a)}$. Thus $\boldsymbol{\sigma} = \boldsymbol{\sigma}^{(v)} + \boldsymbol{\sigma}^{(r)} + \boldsymbol{\sigma}^{(a)}$. The reactive term $\boldsymbol{\sigma}^{(r)} = -P\mathbf{1} + \boldsymbol{\sigma}^{(d)} + \boldsymbol{\sigma}^{(e)}$ consists, in turn, of three contributions: an isotropic pressure P , an *elastic* stress $\sigma_{ij}^{(e)} = -L_p \partial_i \mathbf{Q}_p \odot \partial_j \mathbf{Q}_p$, where L_p is the order parameter stiffness and the symbol \odot denotes a contraction of all matching indices of the two operands and yields a tensor whose rank equates the number of unmatched indices (two in this case). The term $\boldsymbol{\sigma}^{(d)}$ is a *dynamic* stress originating from the reversible coupling between p -atic order and flow and is routinely derived from the fluid's entropy production [37]. Finally, the active stress $\boldsymbol{\sigma}^{(a)}$ can be constructed phenomenologically for arbitrary p values: i.e.

$$\boldsymbol{\sigma}^{(a)} = \sum_p (\alpha_p \nabla^{\otimes p-2} \odot \mathbf{Q}_p + \beta_p [\nabla^{\otimes 2} |\mathbf{Q}_p|^2]) , \quad (5)$$

where the sum over p reflects the possibility of having not only one, but multiple types of p -atic order coexisting within the same system.

Before exploring the consequences of the latter hypothesis, some comment about the physical interpretation of the terms featured in Eq. (5) is in order. The first term on the right-hand side of Eq. (5) is the stress resulting from the contractile or extensile forces exerted at the length scale of individual cells. To illustrate this concept one can assume each cell to exert a p -fold symmetric force complexion (Fig. 1c): i.e. $\mathbf{F}_c = \sum_{k=1}^p \mathbf{F}_k \delta(\mathbf{r} - \mathbf{r}_c - a\boldsymbol{\nu}_k)$ with \mathbf{F}_k the force exerted by a cell at each vertex, \mathbf{r}_c and a respectively the cell's centroid and circumradius and $\boldsymbol{\nu}_k = \cos(\vartheta + 2\pi k/p) \mathbf{e}_x + \sin(\vartheta + 2\pi k/p) \mathbf{e}_y$. Next, assuming $\mathbf{F}_k = f \boldsymbol{\nu}_k$ and expanding the delta function about $a = 0$ yields $\mathbf{F}_c = \sum_{m=0}^{\infty} \mathbf{f}_m$, where

$$\mathbf{f}_m = \nabla^{\otimes m} \odot \left[\frac{(-a)^m f}{m!} \left(\sum_{k=1}^p \boldsymbol{\nu}_k^{\otimes m+1} \right) \delta(\mathbf{r} - \mathbf{r}_c) \right] . \quad (6)$$

Because of the p -fold symmetry of the force complexion $\mathbf{f}_m = \mathbf{0}$ for all even m values, unless $m = p - 1$, whereas odd m values yields, up to symmetrization, $\sum_{k=1}^p \boldsymbol{\nu}_k^{\otimes m+1} \sim \mathbf{1}^{\otimes(m+1)/2}$. Thus, after some algebraic manipulation, one finds $\mathbf{F}_c \approx -apf/2 \nabla[(1 + a^2/8 \nabla^2 + \dots) \delta(\mathbf{r} - \mathbf{r}_c)] + \mathbf{f}_{p-1}$. Finally, taking $\langle \sum_c \mathbf{F}_c \rangle = -\nabla \cdot \mathbf{H}$ gives the following expression for the coarse-grained

stress tensor $\mathbf{H} = \Pi \mathbf{1} + [\Pi]$. That is

$$\Pi = \frac{apf}{2} \left(n + \frac{a^2}{8} \nabla^2 n + \dots \right) , \quad (7a)$$

$$[\Pi] = -\frac{(-a)^{p-1} pf}{\sqrt{2^{p-2}} (p-1)!} \nabla^{p-2} \odot \mathbf{Q}_p , \quad (7b)$$

where $n = \langle \sum_c \delta(\mathbf{r} - \mathbf{r}_c) \rangle$ is the cell number density Eq. (7a) gives the contribution to the pressure P resulting from the isotropic expansion/contraction of the cells, while the deviatoric stress $[\Pi]$ in Eq. (7b) equates the first term of Eq. (5), with $\alpha_p = -(-a)^{p-1} pf / [\sqrt{2^{p-2}} (p-1)!]$.

The second term in Eq. (5), by contrast, expresses the active stress resulting from the spatial variations of the p -atic order parameter. Although similar to the elastic stress $\boldsymbol{\sigma}^{(e)}$, this cannot be derived from a free energy and represents, therefore, a possible contribution to the active stress. Other second order terms can be constructed, but these are not independent on $\partial_i \mathbf{Q}_p \odot \partial_j \mathbf{Q}_p$ and $\nabla^{\otimes 2} |\mathbf{Q}_p|^2$, thus lead to a mere renormalization of the coefficients L_p and β_p .

We now observe that Eq. (5) entails a multiscale hydrodynamic behavior even when a single p value is considered. Such a crossover is expected at length scales larger than $\ell_x = (\alpha_p / \beta_p)^{1/(p-4)}$, where the second term of the right-hand side of Eq. (5) overweights the first term, reflecting the p -fold symmetry of the local active forces. In the presence of multiple types of p -atic order, the p -dependent structure of the active stress renders the multiscale nature of the system enormously more dramatic. To illustrate this crucial point, here we postulate the system to behave as a hexanematic liquid crystal. An experimental test of this hypothesis is reported in Ref. [38]. Formally, such a scenario can be accounted for by simultaneously solving two variants of Eq. (4c), for \mathbf{Q}_2 and \mathbf{Q}_6 . In turn, the interplay between nematic and hexatic order results from a combination of dynamical and energetic effects. The former arise from active flow, which affects the local configuration of both tensor order parameters via the last four terms in Eq. (4c). The latter, instead, can be embedded into the free energy $F = \int d\mathbf{A} (f_2 + f_6 + f_{2,6})$, where

$$f_p = \frac{1}{2} L_p |\nabla \mathbf{Q}_p|^2 + \frac{1}{2} A_p |\mathbf{Q}_p|^2 + \frac{1}{4} B_p |\mathbf{Q}_p|^4 , \quad (8a)$$

$$f_{2,6} = \kappa_{2,6} |\mathbf{Q}_2|^2 |\mathbf{Q}_6|^2 + \chi_{2,6} \mathbf{Q}_2^{\otimes 3} \odot \mathbf{Q}_6 . \quad (8b)$$

Here, A_p and B_p are constants setting the magnitude of the order parameter at the length scale of the short distance cut-off, here assumed to be of the order of the cell size, and $\kappa_{2,6}$ determines the extent to which the magnitude of the hexatic order parameter is influenced by that of the nematic order parameter and vice versa. The constant $\chi_{2,6}$, on the other hand, is analogous to an inherent susceptibility, expressing the propensity of the nematic and hexatic directors towards mutual alignment.

To test the significance of this hypothesis, we next compute the structure factor $S = S(\mathbf{q})$ defined as the Fourier

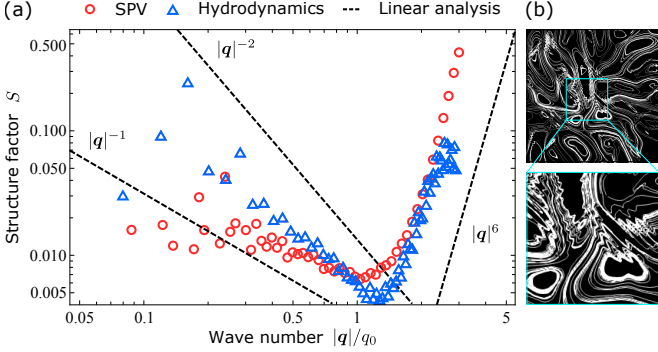


FIG. 2. (a) Structure factor of model-epithelia calculated from the SPV model, Eqs. (1) and (2) (red circles), from the exact numerical solution of Eqs. (4) (blue triangles) and analytically at linear order (dashed lines). The parameters of the SPV model are: $v_0/(\mu/K_A A_0^{3/2}) = 0.5$, $\mathcal{D}_r/(\mu K_p) = 1$ and $p_0 = 3.85$ for a system of 10^4 cells. The wave number is expressed in units of $q_0 = 2\pi/d$, where d the average distance between cells. Both simulations are performed on square domain with periodic boundary and sizes $L_{\text{SPV}}/d = 100$ (SPV model) and $L_H/d = 6400$. (b) Example of the hexanematic flow field obtained from Eqs. (4). The multiscale structure is revealed by the small zig-zag features appearing along the streamlines of the large vortices.

transform of the equal-time correlation function of the density fluctuations, i.e. $\delta\rho = \rho - \rho_0$, about the average density ρ_0 . To this end, we assume for simplicity both the nematic and the hexatic scalar order parameters to be uniform throughout the system and flow alignment effects to be negligible. With these simplifications, whose legitimacy will be assessed *a posteriori*, one can derive from Eq. (4c) the following set of hydrodynamic equations for the fluctuating fields $\boldsymbol{\nu}_2 = \cos\vartheta_2 \mathbf{e}_x + \sin\vartheta_2 \mathbf{e}_y$ and $\boldsymbol{\nu}_6 = \cos\vartheta_6 \mathbf{e}_x + \sin\vartheta_6 \mathbf{e}_y$, expressing the orientation of the nematic and hexatic cell clusters, at the smallest length scale where these can be identified while still being subject to fluctuations. That is

$$\frac{D\vartheta_2}{Dt} = \mathcal{D}_2 \nabla^2 \vartheta_2 + \omega_{xy} + \frac{3\chi_2}{8} \sin 6(\vartheta_2 - \vartheta_6) + \xi_2, \quad (9a)$$

$$\frac{D\vartheta_6}{Dt} = \mathcal{D}_6 \nabla^2 \vartheta_6 + \omega_{xy} + \frac{\chi_6}{24} \sin 6(\vartheta_6 - \vartheta_2) + \xi_6, \quad (9b)$$

where $\mathcal{D}_p = \Gamma_p L_p$ is the rotational diffusion coefficient of the associated p -atic phase, $\chi_p = \Gamma_p \chi_{2,6}$ and $\xi_p = \xi_p(\mathbf{r}, t)$ is a white noise field having zero mean and correlation function $\langle \xi_p(\mathbf{r}, t) \xi_{p'}(\mathbf{r}', t') \rangle = 2 \Xi_p \delta_{pp'} \delta(\mathbf{r} - \mathbf{r}') \delta(t - t')$. Furthermore, we assume viscous forces to be subleading compared to frictional forces originating from the interaction with the substrate, so that $\boldsymbol{v} = (\nabla \cdot \boldsymbol{\sigma})/\zeta$, with the stress tensor

$$\boldsymbol{\sigma} = \boldsymbol{\sigma}_2^{(r)} + \boldsymbol{\sigma}_6^{(r)} + \alpha_2 [\![\boldsymbol{\nu}_2^{\otimes 2}]\!] + \alpha_6 \nabla^{\otimes 4} \odot [\![\boldsymbol{\nu}_6^{\otimes 6}]\!], \quad (10)$$

where $\boldsymbol{\sigma}_p^{(r)}$ is the reactive stress tensor associated with each p -atic phase [37] and we have incorporated the

magnitude of the order parameter in the definition of the constants α_2 and α_6 . Crucially, Eq. (10) entails two length scales, reflecting the distance at which the passive torques originating from the entropic elasticity of the nematic and hexatic phases counterbalance those arising from the active stresses. These are $\ell_2 = \sqrt{L_2/|\alpha_2|}$ (see Ref. [39]) and $\ell_6 = \sqrt{|\alpha_6|/L_6}$.

To fix ideas we first consider the case where the coupling constant $\chi_{2,6} = 0$ (hence $\chi_2 = \chi_6 = 0$), so that the orientations ϑ_2 and ϑ_6 are coupled solely by the flow. In this case, linearizing Eqs. (4a) and (9) and using Eq. (10), gives

$$S = \frac{s_{-2}}{|\mathbf{q}|^2} + s_6 |\mathbf{q}|^6, \quad (11)$$

where $s_{-2} \sim \alpha_2^2$ and $s_6 \sim \alpha_6^2$ [37]. The first term entails the typical giant number density fluctuations associated with the active nematic behavior at the large scale (i.e. $|\mathbf{q}| \rightarrow 0$). This effect is overestimated at the linear order, leading to an inverse quadratic dependence on the wave number $|\mathbf{q}|$ [40], but is generally renormalized by nonlinearities, so that $S \sim |\mathbf{q}|^{-\alpha}$, with $1 < \alpha < 2$ [41, 42]. The last term, by contrast, reflects the 6-fold symmetry characterizing the structure of epithelia at the small length scale ($|\mathbf{q}| \rightarrow \infty$). Finally, switching on the direct coupling between nematic and hexatic order, by taking finite χ_2 and χ_6 values, only affects the system's structure at intermediate scales, without changing neither the small nor the large scale behavior [37].

Fig. 2 shows a plot of the structure factor computed from simulations of the SPV model, Eqs. (1) and (2), and from a numerical integration of Eqs. (4) [43, 44], with none of the simplifications behind Eq. (11). Consistently with our linear analysis, both data sets exhibit two different power-law scaling behaviors at small and large length scales. At small length scales S grows as $|\mathbf{q}|^6$. Conversely, at larger length scales, the structure factor scales like an inverse power law, with exponent compatible with the large scale behavior of “dry” active nematics [42]. Notably, this also occurs for a choice of parameters well in the isotropic phase, consistently with the experimental observations on jammed monolayers of human mammary epithelial MCF-10A cells fluidized by over-expression of the RAB5A protein [45]. The crossover between these different scaling regimes occurs when $\ell_2 \approx \ell_6$, that is for $|\mathbf{q}|/q_0 \approx 1$ with respect to the parameters used in Fig. 2.

In conclusions, we have introduced a continuum model of collectively migrating layers of epithelial cells, built upon a recent generalization of the hydrodynamic theory of p -atic liquid crystals [34, 35]. This approach allows one to account for arbitrary discrete rotational symmetries, thereby going beyond existing hydrodynamic theories of epithelia (see e.g. Refs. [20–26]), where the algebraic structure of the hydrodynamic variables renders impossible to account for liquid crystal order other than isotropic (i.e. $p = 0$), polar (i.e. $p = 1$) or nematic (i.e. $p = 2$). Upon computing the static structure factor and comparing this with the outcome of a popular

cell-resolved model, i.e. the SPV model [7], we have shown that migrating epithelial layers may in fact comprise both nematic and hexatic (i.e. $p = 6$) order, co-existing at different length scales. Although the consequences of such a remarkable versatility are yet to be explored, we expect hexatic order to be relevant for short-scale remodelling events, where the local nature of hexatic order, combined with the rich dynamics of hexatic defects [33, 46], may mediate processes such as cell intercalations and the rearrangement of multicellular *rosettes* (see e.g. Refs. [47, 48]). Such a local motion, in turn, may be coordinated at the large scale by the underlying nematic order, giving rise to a persistent unidirectional flow, such as that observed during wound healing and cancer progression [1]. Furthermore, the existence of multiscale liquid crystal order echoes the most recent understanding of phenotypic plasticity in tissues, according to which the epithelial (i.e. solid-like) and mesenchymal (i.e. liquid-like) states represent the two ends of a spectrum of intermediate phenotypes [49]. These intermediate states display distinctive cellular characteristics,

including adhesion, motility, stemness and, in the case of cancer cells, invasiveness, drug resistance etc. Can multiscale liquid crystal order help understanding how the biophysical properties of tissues vary along the epithelial-mesenchymal spectrum? This and related questions will be addressed in the near future.

ACKNOWLEDGMENTS

We are indebted with Massimo Pica Ciamarra and David Nelson for insightful discussions. This work is supported by the ERC-CoG grant HexaTissue (L.N.C. and L.G.) and by Netherlands Organization for Scientific Research (NWO/OCW) as part of the research program “The active matter physics of collective metastasis” with project number Science-XL 2019.022 (J.-M.A.-C.). Part of this work was carried out on the Dutch national e-infrastructure with the support of SURF through the Grant 2021.028 for computational time.

[1] P. Friedl and D. Gilmour, *Nat. Rev. Mol. Cell Bio.* **10**, 445 (2009).

[2] X. Serra-Picamal, V. Conte, R. Vincent, E. Anon, D. T. Tambe, E. Bazellieres, J. P. Butler, J. J. Fredberg and X. Trepat, *Nat. Phys.* **8**, 628 (2012).

[3] A. Haeger, S. Alexander, M. Vullings, F. M. P. Kaiser, C. Veelken, U. Flucke, G. E. Koehl, M. Hirschberg, M. Flentje, R. M. Hoffman, E. K. Geissler, S. Kissler, P. Friedl, *J. Exp. Med.* **6**, 217, e20181184 (2020)

[4] T. Nagai and H. Honda, *Philos. Mag. B* **81**, 699 (2001).

[5] R. Farhadifar, J.-C. Röper, B. Aigouy, S. Eaton and F. Jülicher, *Curr. Biol.* **17**, 2095 (2007).

[6] D. Bi, J. H. Lopez, J. M. Schwarz and M. Lisa Manning, *Nat. Phys.* **11**, 1074 (2015).

[7] D. Bi, X. Yang, M. C. Marchetti and M. L. Manning, *Phys. Rev. X* **6**, 021011 (2016).

[8] A. Boromand, A. Signoriello, F. Ye, C. S. O’Hern and M. D. Shattuck *Phys. Rev. Lett.* **121**, 248003 (2018).

[9] R. Mueller, J. M. Yeomans, and A. Doostmohammadi, *Phys. Rev. Lett.* **122**, 048004 (2019).

[10] B. Loewe, M. Chiang, D. Marenduzzo and M. C. Marchetti *Phys. Rev. Lett.* **125**, 038003 (2020).

[11] S. Monfared, G. Ravichandran, J. E. Andrade and A. Doostmohammadi, *arXiv:2108.07657* (2021).

[12] F. Graner, B. Dollet, C. Raufaste and P. Marmottant, *Eur. Phys. J. E* **25**, 349 (2008).

[13] P. Marmottant, C. Raufaste and F. Graner, *Eur. Phys. J. E* **25**, 371 (2008).

[14] H. Honda, *J. Theor. Biol.* **72**, 523 (1978).

[15] J. A. Park, J. Kim, D. Bi, *et al.*, *Nat. Mater.* **14**, 1040 (2015).

[16] L. Atia, D. Bi, Y. Sharma, *et al.*, *Nat. Phys.* **14**, 613 (2018).

[17] Y.-W. Li and M. Pica Ciamarra, *Phys. Rev. Materials* **2**, 045602 (2018).

[18] A. Pasupalak, Y.-W. Li, R. Ni and M. Pica Ciamarra, *Soft Matter* **16**, 3914 (2020).

[19] M. Durand and J. Heu, *Phys. Rev. Lett.* **123**, 188001 (2019).

[20] J. Ranft, M. Basan, J. Elgeti, J.-F. Joanny, J. Prost and F. Jülicher, *Proc. Natl. Acad. Sci. U.S.A.* **107**, 20863 (2010).

[21] M. Popović, A. Nandi, M. Merkel, R. Etournay, S. Eaton, F. Jülicher and G. Salbreux, *New J. Phys.* **19**, 033006 (2017).

[22] C. Pérez-González, R. Alert, C. Blanch-Mercader, M. Gómez-González, T. Kolodziej, E. Bazellieres, J. Casademunt and X. Trepat, *Nat. Phys.* **15**, 79 (2019).

[23] S. Ishihara, P. Marcq and K. Sugimura, *Phys. Rev. E* **96**, 022418 (2017).

[24] M. Czajkowski, D. Bi, M. L. Manning and M. C. Marchetti, *Soft Matter* **14**, 5628 (2018).

[25] A. Hernandez and M. C. Marchetti, *Phys. Rev. E* **103**, 032612 (2021).

[26] D. Grossman, J.-F. Joanny, *arXiv:2108.05326* (2021).

[27] G. Duclos, C. Blanch-Mercader, V. Yashunsky, G. Salbreux, J.-F. Joanny, J. Prost and P. Silberzan, *Nat. Phys.* **14**, 728 (2018).

[28] C. Blanch-Mercader, V. Yashunsky, S. Garcia, G. Duclos, L. Giomi and P. Silberzan, *Phys. Rev. Lett.* **120**, 208101 (2018).

[29] T. B. Saw, A. Doostmohammadi, V. Nier, L. Kocgozlu, S. Thampi, Y. Toyama, P. Marcq, C. T. Lim, J. M. Yeomans and B. Ladoux, *Nature* **544**, 212 (2017).

[30] K. Kawaguchi, R. Kageyama and M. Sano, *Nature* **545**, 327 (2017).

[31] L. Balasubramaniam, A. Doostmohammadi, T. B. Saw, G. H. N. S. Narayana, R. Mueller, T. Dang, M. Thomas, S. Gupta, S. Sonam, A. S. Yap, Y. Toyama, R.-M. Mége, J. M. Yeomans and B. Ladoux, *Nat. Mater.* **20**, 1156 (2021).

[32] A. Zippelius, *Phys. Rev. A* **22**, 732 (1980).

[33] A. Zippelius, B. I. Halperin, and D. R. Nelson, *Phys. Rev. B* **22**, 2514 (1980).

- [34] L. Giomi, J. Toner and N. Sarkar, [arXiv:2111.04720 \(2021\)](https://arxiv.org/abs/2111.04720).
- [35] L. Giomi, J. Toner and N. Sarkar, [arXiv:2106.11957 \(2021\)](https://arxiv.org/abs/2106.11957).
- [36] S. Hess, *Tensors for physics* (Springer International Publishing, New York NY, 2015).
- [37] Supplementary information.
- [38] J.-M. Armengol-Collado, L. N. Carenza, J. Eckert, D. Krommydas, and L. Giomi, *in preparation* (2022).
- [39] L. Giomi, *Phys. Rev. X* **5**, 031003 (2015).
- [40] S. Ramaswamy, R. Aditi Simha and J. Toner, *Europhys. Lett.* **62**, 196 (2003).
- [41] S. Shankar, S. Ramaswamy and M. Cristina Marchetti *Phys. Rev. E* **97**, 012707 (2018).
- [42] H. Chaté, *Annu. Rev. Condens. Matter Phys.* **11**, 189 (2020).
- [43] L. N. Carenza, G. Gonnella, A. Lamura, G. Negro and A. Tiribocchi *Eur. Phys. J. E* **42**, 81 (2019).
- [44] L. N. Carenza, L. Biferale and G. Gonnella *Eur. Phys. Lett.* **132**, 44003 (2020).
- [45] F. Giavazzi, C. Malinverno, S. Corallino, F. Ginelli, G. Scita and R. Cerbino, *J. Phys. D: Appl. Phys.* **50**, 384003 (2017).
- [46] A. Amir and D. R. Nelson, *Proc. Natl. Acad. Sci* **109**, 9833 (2012).
- [47] J. T. Blankenship, S. T. Backovic, J. S. P. Sanny, O. Weitz and J. A. Zallen, *Dev. Cell* **11**, 459 (2006).
- [48] M. Rauzi, *Phil. Trans. R. Soc. B*, **375**, 20190552 (2020).
- [49] Y. Zhang and R. A. Weinberg, *Front. Med.* **12**, 361 (2018).

Hydrodynamics and multiscale order in confluent epithelia: Supplementary information

Josep-Maria Armengol-Collado,^{1,*} Livio N. Carenza,^{1,*} and Luca Giomi^{1,†}

¹*Instituut-Lorentz, Universiteit Leiden, P.O. Box 9506, 2300 RA Leiden, The Netherlands*

S1. REMARKS ON EQ. (10)

As explained in the main text, the stress tensor of our model epithelia consists of the following three terms: $\boldsymbol{\sigma} = \boldsymbol{\sigma}^{(v)} + \boldsymbol{\sigma}^{(r)} + \boldsymbol{\sigma}^{(a)}$. The viscous and active stress tensors are given in the main text. The reactive stress tensor is further decomposed as $\boldsymbol{\sigma}^{(r)} = -P\mathbb{1} + \boldsymbol{\sigma}^{(e)} + \boldsymbol{\sigma}^{(d)}$. The dynamic stress $\boldsymbol{\sigma}^{(d)}$ has been calculated in Refs. [32,33] and is given by

$$\sigma_{ij}^{(d)} = -\bar{\lambda}_p \mathbf{Q}_p \odot \mathbf{H}_p \delta_{ij} + (-1)^{p-1} \lambda_p \partial_{k_1 k_2 \dots k_{p-2}}^{p-2} H_{k_1 k_2 \dots i j} + \frac{p}{2} (Q_{k_1 k_2 \dots i} H_{k_1 k_2 \dots j} - H_{k_1 k_2 \dots i} Q_{k_1 k_2 \dots j}) . \quad (\text{S1})$$

Under the assumptions of uniform order parameter, i.e. $|\mathbf{Q}_p|^2 = |\Psi_p|^2/2 = \text{const}$, and negligible flow alignment effects, the first two terms in Eq. (S1) can be ignored, whereas the third term, combined with the isotropic pressure and the elastic stress $\boldsymbol{\sigma}^{(e)}$ yields the standard reactive stress tensor computed by Zippelius *et al.* in Refs. [30,31]. That is

$$\boldsymbol{\sigma}^{(r)} = -P\mathbb{1} + \frac{K_p}{2} \boldsymbol{\varepsilon} \nabla^2 \theta - K_p \nabla \theta \otimes \nabla \theta , \quad (\text{S2})$$

where K_p is the orientational stiffness of the p -atic phase, related to the order parameter stiffness by

$$K_p = \frac{p^2 |\Psi_p|^2}{2} L_p \quad (\text{S3})$$

and $\boldsymbol{\varepsilon}$ is the two-dimensional antisymmetric tensor, with $\varepsilon_{xy} = -\varepsilon_{yx} = 1$ and $\varepsilon_{xx} = \varepsilon_{yy} = 0$.

S2. LINEARIZED HYDRODYNAMICS

The hydrodynamic equations (4a) and (9) are given, at the linear order in $\delta\rho = \rho - \rho_0$, $\delta\vartheta_2 = \vartheta_2 - \theta_2$, $\delta\vartheta_6 = \vartheta_6 - \theta_6$ and $\mathbf{v} = \nabla \cdot \boldsymbol{\sigma}/\varsigma$ by

$$\partial_t \delta\rho = \mathcal{D}_0 \nabla^2 \delta\rho - \rho_0 \nabla \cdot \mathbf{v} , \quad (\text{S4a})$$

$$\partial_t \delta\vartheta_2 = \mathcal{D}_2 \nabla^2 \delta\vartheta_2 + \frac{1}{2} \mathbf{e}_z \cdot (\nabla \times \mathbf{v}) + \frac{9}{4} \chi_2 (\delta\vartheta_2 - \delta\vartheta_6) + \xi_2 , \quad (\text{S4b})$$

$$\partial_t \delta\vartheta_6 = \mathcal{D}_6 \nabla^2 \delta\vartheta_6 + \frac{1}{2} \mathbf{e}_z \cdot (\nabla \times \mathbf{v}) + \frac{1}{4} \chi_6 (\delta\vartheta_6 - \delta\vartheta_2) + \xi_6 . \quad (\text{S4c})$$

The linearized flow velocity, on the other hand, can be computed, up to divergenceless terms which do not contribute to the dynamics of the density fluctuations, in the form

$$\begin{aligned} \mathbf{v} = & \frac{1}{\varsigma} \left[\alpha_2 \partial_y \delta\vartheta_2 + \frac{3}{2} \alpha_6 \left(\partial_y^4 - 5 \partial_x^2 \partial_y^2 + \frac{5}{2} \partial_x^4 \right) \partial_y \delta\vartheta_6 \right] \mathbf{e}_x \\ & + \frac{1}{\varsigma} \left[\alpha_2 \partial_x \delta\vartheta_2 + \frac{3}{2} \alpha_6 \left(\partial_x^4 - 5 \partial_x^2 \partial_y^2 + \frac{5}{2} \partial_y^4 \right) \partial_x \delta\vartheta_6 \right] \mathbf{e}_y , \end{aligned} \quad (\text{S5})$$

* These authors contributed equally.

† giomi@lorentz.leidenuniv.nl

Using Eq. (S5) one can cast Eqs. (S6) in the following form:

$$\partial_t \begin{bmatrix} \delta\rho \\ \delta\vartheta_2 \\ \delta\vartheta_6 \end{bmatrix} = \mathbf{M} \cdot \begin{bmatrix} \delta\rho \\ \delta\vartheta_2 \\ \delta\vartheta_6 \end{bmatrix} + \begin{bmatrix} 0 \\ \xi_2 \\ \xi_6 \end{bmatrix}, \quad (\text{S6})$$

where we have introduced the matrix

$$\mathbf{M} = \begin{bmatrix} \mathcal{D}_0 \nabla^2 & -2\alpha_2 \rho_0 \partial_x \partial_y & -\frac{3}{2} \alpha_6 \rho_0 (3\partial_x^5 \partial_y - 10\partial_x^3 \partial_y^3 + 3\partial_x \partial_y^5) \\ 0 & \mathcal{D}_2 \nabla^2 + \frac{9}{4} \chi_2 + \frac{1}{2} \alpha_2 (\partial_x^2 - \partial_y^2) & -\frac{9}{4} \chi_2 + \frac{3}{8} \alpha_6 (\partial_x^6 - 15\partial_x^4 \partial_y^2 + 15\partial_x^2 \partial_y^4 - \partial_y^6) \\ 0 & -\frac{1}{4} \chi_6 + \frac{1}{2} \alpha_2 (\partial_x^2 - \partial_y^2) & \mathcal{D}_6 \nabla^2 + \frac{1}{4} \chi_6 + \frac{3}{8} \alpha_6 (\partial_x^6 - 15\partial_x^4 \partial_y^2 + 15\partial_x^2 \partial_y^4 - \partial_y^6) \end{bmatrix}. \quad (\text{S7})$$

Equivalently, Eq. (S6) can be expressed in Fourier space as

$$-i\omega \begin{bmatrix} \delta\hat{\rho} \\ \delta\hat{\vartheta}_2 \\ \delta\hat{\vartheta}_6 \end{bmatrix} = \hat{\mathbf{M}} \cdot \begin{bmatrix} \delta\hat{\rho} \\ \delta\hat{\vartheta}_2 \\ \delta\hat{\vartheta}_6 \end{bmatrix} + \begin{bmatrix} 0 \\ \hat{\xi}_2 \\ \hat{\xi}_6 \end{bmatrix}, \quad (\text{S8})$$

where $\delta\hat{\rho} = \delta\hat{\rho}(\mathbf{q}, \omega)$, $\delta\hat{\vartheta}_2 = \delta\hat{\vartheta}_2(\mathbf{q}, \omega)$ and $\delta\hat{\vartheta}_6 = \delta\hat{\vartheta}_6(\mathbf{q}, \omega)$ are the Fourier amplitudes associated with the modes of frequency ω and wave vector \mathbf{q} of the fields $\delta\rho$, $\delta\vartheta_2$ and $\delta\vartheta_6$ and

$$\hat{\mathbf{M}} = \begin{bmatrix} -\mathcal{D}_0 |\mathbf{q}|^2 & 2\alpha_2 \rho_0 q_x q_y & \frac{3}{2} \alpha_6 \rho_0 (3q_x^5 q_y - 10q_x^3 q_y^3 + 3q_x q_y^5) \\ 0 & -\mathcal{D}_2 |\mathbf{q}|^2 + \frac{9}{4} \chi_2 - \frac{1}{2} \alpha_2 (q_x^2 - q_y^2) & -\frac{9}{4} \chi_2 - \frac{3}{8} \alpha_6 (q_x^6 - 15q_x^4 q_y^2 + 15q_x^2 q_y^4 - q_y^6) \\ 0 & -\frac{1}{4} \chi_6 - \frac{1}{2} \alpha_2 (q_x^2 - q_y^2) & -\mathcal{D}_6 |\mathbf{q}|^2 + \frac{1}{4} \chi_6 - \frac{3}{8} \alpha_6 (q_x^6 - 15q_x^4 q_y^2 + 15q_x^2 q_y^4 - q_y^6) \end{bmatrix}. \quad (\text{S9})$$

S3. DERIVATION OF EQ. (11)

The static structure factor can be expressed in integral form as

$$S = \int_{-\infty}^{\infty} \frac{d\omega}{2\pi} S(\mathbf{q}, \omega), \quad (\text{S10})$$

where the dynamic structure factor $S(\mathbf{q}, \omega)$, can be calculated from the correlation function

$$\langle \delta\hat{\rho}(\mathbf{q}, \omega) \delta\hat{\rho}(\mathbf{q}', \omega') \rangle = (2\pi)^{d+1} S(\mathbf{q}, \omega) \delta(\mathbf{q} + \mathbf{q}') \delta(\omega + \omega'), \quad (\text{S11})$$

with $d = 2$ the spatial dimension. To compute the left-hand side of Eq. (S11) one can solve Eq. (S8) with respect to $\delta\hat{\rho}$, $\delta\hat{\vartheta}_2$ and $\delta\hat{\vartheta}_6$. This gives

$$\delta\hat{\rho} = -\frac{\xi_2 \left[\hat{M}_{\rho\vartheta_2} (\omega - i\hat{M}_{\vartheta_6\vartheta_6}) + i\hat{M}_{\rho\vartheta_6} \hat{M}_{\vartheta_6\vartheta_2} \right] + \xi_6 \left[\hat{M}_{\rho\vartheta_6} (\omega - i\hat{M}_{\vartheta_2\vartheta_2}) + i\hat{M}_{\rho\vartheta_2} \hat{M}_{\vartheta_2\vartheta_6} \right]}{(\omega - i\hat{M}_{\rho\rho}) \left[\omega^2 - i\omega(\hat{M}_{\vartheta_2\vartheta_2} + \hat{M}_{\vartheta_6\vartheta_6}) - \hat{M}_{\vartheta_2\vartheta_2} \hat{M}_{\vartheta_6\vartheta_6} + \hat{M}_{\vartheta_2\vartheta_6} \hat{M}_{\vartheta_6\vartheta_2} \right]}, \quad (\text{S12a})$$

$$\delta\hat{\vartheta}_2 = \frac{\xi_2 (i\omega + \hat{M}_{\vartheta_6\vartheta_6}) - \xi_6 \hat{M}_{\vartheta_2\vartheta_6}}{\left[\omega^2 - i\omega(\hat{M}_{\vartheta_2\vartheta_2} + \hat{M}_{\vartheta_6\vartheta_6}) - \hat{M}_{\vartheta_2\vartheta_2} \hat{M}_{\vartheta_6\vartheta_6} + \hat{M}_{\vartheta_2\vartheta_6} \hat{M}_{\vartheta_6\vartheta_2} \right]}, \quad (\text{S12b})$$

$$\delta\hat{\vartheta}_6 = \frac{\xi_6 (i\omega + \hat{M}_{\vartheta_2\vartheta_2}) - \xi_2 \hat{M}_{\vartheta_6\vartheta_2}}{\left[\omega^2 - i\omega(\hat{M}_{\vartheta_2\vartheta_2} + \hat{M}_{\vartheta_6\vartheta_6}) - \hat{M}_{\vartheta_2\vartheta_2} \hat{M}_{\vartheta_6\vartheta_6} + \hat{M}_{\vartheta_2\vartheta_6} \hat{M}_{\vartheta_6\vartheta_2} \right]}. \quad (\text{S12c})$$

Next, using Eqs. (S10), (S11), (S12a) and taking into account that

$$\langle \xi_p(\mathbf{q}, \omega) \xi_{p'}(\mathbf{q}, \omega') \rangle = (2\pi)^{d+1} (2\Xi_p) \delta_{pp'} \delta(\mathbf{q} + \mathbf{q}') \delta(\omega + \omega'), \quad (\text{S13})$$

gives the following expression for the static structure factor:

$$S = \int_{-\infty}^{\infty} \frac{d\omega}{\pi} \frac{\Xi_2 g_2(\omega) + \Xi_6 g_6(\omega)}{|h(\omega)|^2} , \quad (\text{S14})$$

where we have set

$$g_2(\omega) = (\hat{M}_{\rho\vartheta_2}\omega)^2 + (\hat{M}_{\rho\vartheta_6}\hat{M}_{\vartheta_6\vartheta_2} - \hat{M}_{\rho\vartheta_2}\hat{M}_{\vartheta_6\vartheta_6})^2 , \quad (\text{S15a})$$

$$g_6(\omega) = (\hat{M}_{\rho\vartheta_6}\omega)^2 + (\hat{M}_{\rho\vartheta_2}\hat{M}_{\vartheta_2\vartheta_6} - \hat{M}_{\rho\vartheta_6}\hat{M}_{\vartheta_2\vartheta_2})^2 , \quad (\text{S15b})$$

$$h(\omega) = (\omega - i\hat{M}_{\rho\rho}) \left[\omega^2 - i\omega(\hat{M}_{\vartheta_2\vartheta_2} + \hat{M}_{\vartheta_6\vartheta_6}) - \hat{M}_{\vartheta_2\vartheta_2}\hat{M}_{\vartheta_6\vartheta_6} + \hat{M}_{\vartheta_2\vartheta_6}\hat{M}_{\vartheta_6\vartheta_2} \right] . \quad (\text{S15c})$$

The integral over ω can be computed using the residue theorem upon computing the roots of the complex third-order polynomial h . To make progress, we express

$$|h(\omega)|^2 = (\omega^2 + \omega_1^2)(\omega^2 + \omega_2^2)(\omega^2 + \omega_3^2) , \quad (\text{S16})$$

where ω_1 , ω_2 and ω_3 are given by

$$\omega_1 = \hat{M}_{\rho\rho} , \quad (\text{S17a})$$

$$\omega_2 = \frac{1}{2} \left(\hat{M}_{\vartheta_2\vartheta_2} + \hat{M}_{\vartheta_6\vartheta_6} - \sqrt{(\hat{M}_{\vartheta_2\vartheta_2} - \hat{M}_{\vartheta_6\vartheta_6})^2 + 4\hat{M}_{\vartheta_2\vartheta_6}\hat{M}_{\vartheta_6\vartheta_2}} \right) , \quad (\text{S17b})$$

$$\omega_3 = \frac{1}{2} \left(\hat{M}_{\vartheta_2\vartheta_2} + \hat{M}_{\vartheta_6\vartheta_6} + \sqrt{(\hat{M}_{\vartheta_2\vartheta_2} - \hat{M}_{\vartheta_6\vartheta_6})^2 + 4\hat{M}_{\vartheta_2\vartheta_6}\hat{M}_{\vartheta_6\vartheta_2}} \right) . \quad (\text{S17c})$$

The integrand on the right-hand side of Eq. (S14) has, therefore, three pairs of purely imaginary poles: i.e. $\pm i|\omega_1|$, $\pm i|\omega_2|$ and $\pm i|\omega_3|$. Next, turning the integration range to an infinite semicircular contour on the complex upper half-plane and summing the associated residues gives, after lengthy algebraic manipulations

$$S = \frac{\Xi_2 \left[\Omega_1 \hat{M}_{\rho\vartheta_2}^2 + \Omega_2 (\hat{M}_{\rho\vartheta_6}\hat{M}_{\vartheta_6\vartheta_2} - \hat{M}_{\rho\vartheta_2}\hat{M}_{\vartheta_6\vartheta_6})^2 \right] + \Xi_6 \left[\Omega_1 \hat{M}_{\rho\vartheta_6}^2 + \Omega_2 (\hat{M}_{\rho\vartheta_2}\hat{M}_{\vartheta_2\vartheta_6} - \hat{M}_{\rho\vartheta_6}\hat{M}_{\vartheta_2\vartheta_2})^2 \right]}{\Omega_1 \Omega_2 \Omega_3 - \Omega_1^2} , \quad (\text{S18})$$

where we have set

$$\Omega_1 = |\omega_1||\omega_2||\omega_3| , \quad (\text{S19a})$$

$$\Omega_2 = |\omega_1| + |\omega_2| + |\omega_3| , \quad (\text{S19b})$$

$$\Omega_3 = |\omega_1||\omega_2| + |\omega_1||\omega_3| + |\omega_2||\omega_3| . \quad (\text{S19c})$$

Now, in the case where $\chi_2 = \chi_6 = 0$, $\hat{M}_{\vartheta_2\vartheta_6} = \hat{M}_{\vartheta_6\vartheta_2} = 0$ and Eq. (S18) simplifies to

$$S = \frac{\Xi_2 \hat{M}_{\rho\vartheta_2}^2}{|\hat{M}_{\rho\rho}||\hat{M}_{\vartheta_2\vartheta_2}| \left(|\hat{M}_{\rho\rho}| + |\hat{M}_{\vartheta_2\vartheta_2}| \right)} + \frac{\Xi_6 \hat{M}_{\rho\vartheta_6}^2}{|\hat{M}_{\rho\rho}||\hat{M}_{\vartheta_6\vartheta_6}| \left(|\hat{M}_{\rho\rho}| + |\hat{M}_{\vartheta_6\vartheta_6}| \right)} . \quad (\text{S20})$$

Finally, taking for simplicity $q_x = q_y = |\mathbf{q}|/\sqrt{2}$ gives

$$\begin{aligned} \hat{M}_{\rho\rho} &= -\mathcal{D}_0 |\mathbf{q}|^2 , & \hat{M}_{\vartheta_2\vartheta_2} &= -\mathcal{D}_2 |\mathbf{q}|^2 , & \hat{M}_{\vartheta_6\vartheta_6} &= -\mathcal{D}_6 |\mathbf{q}|^2 , \\ \hat{M}_{\rho\vartheta_2} &= \alpha_2 \rho_0 |\mathbf{q}|^2 , & \hat{M}_{\rho\vartheta_6} &= -\frac{3}{4} \alpha_6 \rho_0 |\mathbf{q}|^6 , \end{aligned}$$

from which we recover Eq. (11) in the main text, with

$$s_{-2} = \frac{(\alpha_2 \rho_0)^2}{\mathcal{D}_0 \mathcal{D}_2 (\mathcal{D}_0 + \mathcal{D}_2)} , \quad s_6 = \frac{\left(\frac{3}{4} \alpha_6 \rho_0\right)^2}{\mathcal{D}_0 \mathcal{D}_6 (\mathcal{D}_0 + \mathcal{D}_6)} . \quad (\text{S21})$$

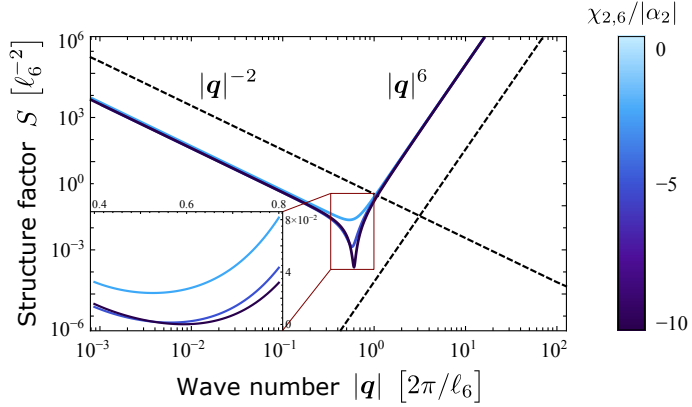


Fig. S1. Structure factor as given by Eq. (S22) for three $\chi_{2,6}$ values and $\Gamma_2 = \Gamma_6$. Compared to the case where the hexatic and nematic directors are coupled solely by the active flow (i.e. $\chi_{2,6} = 0$), the static coupling entailed in the parameter $\chi_{2,6}$ exclusively affects the intermediate length scales. In this example, the typical length scale associated with the nematic active stress, i.e. $\ell_2 = \sqrt{L_2/|\alpha_2|}$ is ten times larger than the corresponding hexatic scale, i.e. $\ell_6 = \sqrt{|\alpha_6|/L_6}$, thereby producing features at wave numbers of order $(10\ell_6)^{-1}$.

For finite χ_2 and χ_6 values, taking again $q_x = q_y = |\mathbf{q}|/\sqrt{2}$ gives

$$\begin{aligned} \hat{M}_{\rho\rho} &= -\mathcal{D}_0|\mathbf{q}|^2, & \hat{M}_{\vartheta_2\vartheta_2} &= -\mathcal{D}_2|\mathbf{q}|^2 + \frac{9}{4}\chi_2, & \hat{M}_{\vartheta_6\vartheta_6} &= -\mathcal{D}_6|\mathbf{q}|^2 + \frac{1}{4}\chi_6, \\ \hat{M}_{\rho\vartheta_2} &= \alpha_2\rho_0|\mathbf{q}|^2, & \hat{M}_{\rho\vartheta_6} &= -\frac{3}{4}\alpha_6\rho_0|\mathbf{q}|^6, & \hat{M}_{\vartheta_2\vartheta_6} &= -\frac{9}{4}\chi_2, & \hat{M}_{\vartheta_6\vartheta_2} &= -\frac{1}{4}\chi_6. \end{aligned}$$

Using these in combination with Eqs. (S17), (S18) and (S19) gives the following expression for the generic structure factor:

$$S = \frac{(\alpha_2\rho_0)^2}{\mathcal{D}_0\mathcal{P}} (\Xi_2\mathcal{N}_2 + \Xi_6\mathcal{N}_6) + \frac{\alpha_2\alpha_6\rho_0^2}{\mathcal{D}_0\mathcal{P}} (\Xi_2\mathcal{X}_2 + \Xi_6\mathcal{X}_6) + \frac{(\alpha_6\rho_0)^2}{\mathcal{D}_0\mathcal{P}} (\Xi_2\mathcal{H}_2 + \Xi_6\mathcal{H}_6), \quad (\text{S22})$$

where we have called

$$\begin{aligned} \mathcal{N}_2 &= [4(\mathcal{D}_2 + \mathcal{D}_6)|\mathbf{q}|^2 - 9\chi_2 - \chi_6] (\chi_6 - 4\mathcal{D}_6|\mathbf{q}|^2)^2 |\mathbf{q}|^{-2} \\ &+ 4\mathcal{D}_0 \{ 4\mathcal{D}_6 [4(\mathcal{D}_2 + \mathcal{D}_6)|\mathbf{q}|^2 - 9\chi_2] - 4\chi_6(\mathcal{D}_2 + 2\mathcal{D}_6) \} |\mathbf{q}|^2 + 4\mathcal{D}_0\chi_6^2, \end{aligned} \quad (\text{S23a})$$

$$\mathcal{N}_6 = 81\chi_2^2 [4(\mathcal{D}_0 + \mathcal{D}_2 + \mathcal{D}_6)|\mathbf{q}|^2 - 9\chi_2 - \chi_6] |\mathbf{q}|^{-2}, \quad (\text{S23b})$$

$$\mathcal{H}_2 = \frac{9}{16}\chi_6^2 [4(\mathcal{D}_0 + \mathcal{D}_2 + \mathcal{D}_6)|\mathbf{q}|^2 - 9\chi_2 - \chi_6] |\mathbf{q}|^6, \quad (\text{S23c})$$

$$\begin{aligned} \mathcal{H}_6 &= \frac{9}{16} (4\mathcal{D}_2|\mathbf{q}|^2 - 9\chi_2) [4(\mathcal{D}_0 + \mathcal{D}_2)|\mathbf{q}|^2 - 9\chi_2] [4(\mathcal{D}_2 + \mathcal{D}_6)|\mathbf{q}|^2 - 9\chi_2] |\mathbf{q}|^6 \\ &- \frac{9}{16}\chi_6 \left[(4\mathcal{D}_2|\mathbf{q}|^2 - 9\chi_2)^2 + 16\mathcal{D}_0\mathcal{D}_2|\mathbf{q}|^4 \right] |\mathbf{q}|^6, \end{aligned} \quad (\text{S23d})$$

$$\mathcal{X}_2 = \frac{3}{2}\chi_6 (4\mathcal{D}_6|\mathbf{q}|^2 - \chi_6) [4(\mathcal{D}_0 + \mathcal{D}_2 + \mathcal{D}_6)|\mathbf{q}|^2 - 9\chi_2 - \chi_6] |\mathbf{q}|^2, \quad (\text{S23e})$$

$$\mathcal{X}_6 = \frac{27}{2}\chi_2 (4\mathcal{D}_2|\mathbf{q}|^2 - 9\chi_2) [4(\mathcal{D}_0 + \mathcal{D}_2 + \mathcal{D}_6)|\mathbf{q}|^2 - 9\chi_2 - \chi_6] |\mathbf{q}|^2, \quad (\text{S23f})$$

$$\begin{aligned} \mathcal{P} &= [\mathcal{D}_2 (4\mathcal{D}_6|\mathbf{q}|^2 - \chi_6) - 9\mathcal{D}_6\chi_2] [4(\mathcal{D}_2 + \mathcal{D}_6)|\mathbf{q}|^2 - 9\chi_2 - \chi_6] \\ &\times \{ (\mathcal{D}_0 + \mathcal{D}_6) [4(\mathcal{D}_0 + \mathcal{D}_2)|\mathbf{q}|^2 - 9\chi_2] - (\mathcal{D}_0 + \mathcal{D}_2)\chi_6 \}, \end{aligned} \quad (\text{S23g})$$

under the assumption that $\chi_2 < 0$ and $\chi_6 < 0$. Unfortunately the structure factor, Eq. (S22), cannot be further simplified. As explained in the main text, however, the static coupling between the nematic and the hexatic order parameter tensor affects the structure of the system only at intermediate length scales, without changing neither one of the asymptotic behaviors. This can be better appreciated from Fig. S1, where the structure factor is plotted for various χ_2 and χ_6 values.

S4. NUMERICAL MODEL FOR INTEGRATION OF HYDRODYNAMICS IN EQUATIONS (4)

The dynamical equations have been integrated by means of a hybrid lattice Boltzmann (LB) method, where the hydrodynamics is solved through a *predictor-corrector* LB algorithm, while the dynamics of the order parameter has been treated with a predictor-corrector finite-difference Euler approach implementing a first-order upwind scheme and second-order accurate stencils for the computation of spacial derivatives [41,42]. The numerical code has been parallelized by means of Message Passage Interface (MPI), by dividing the computational domain in slices and by implementing the ghost-cell method to compute derivatives on the boundary of the computational subdomains. Runs have been performed using 64 CPUs in two-dimensional geometries, on a computational box of size 256^2 and 512^2 , for at least 1.5×10^7 lattice Boltzmann iterations (corresponding to $\sim 21d$ and $\sim 84d$ of CPU-time, respectively for the smaller and larger computational boxes). Periodic boundary conditions have been imposed. The director fields (for both $p = 2$ and $p = 6$) have been randomly initialized. The initial density field is assumed to be uniform with $\rho = 2.0$ everywhere. The model parameters used for simulations are: $\mathcal{D}_0 = 0.001$, $\eta = \zeta = 1.66$, $\lambda_2 = \lambda_6 = 1.1$, $\nu_2 = \nu_6 = 0.0$, $\Gamma_2 = 0.4$, $A_2 = -B_2 = -0.04$, $L_2 = 0.04$, $\Gamma_6 = 0.4$, $A_6 = -B_6 = -0.004$, $L_6 = 0.004$, $\kappa_{2,6} = \xi_{2,6} = -0.004$. Nematic activity α_2 has been varied in the range $-0.02 \leq \alpha_2 \leq -0.0005$ and hexatic activity α_6 in the range $-0.050 \leq \alpha_6 \leq 0.050$. We set the active parameters β_2 and $\beta_6 = 0$.